TABLE OF CONTENTS – CHAPTER 6 through 6.4

CHAPTER 6
CONCEPTUAL DESIGN SELECTION AND DESCRIPTION

This chapter describes the selection of the specific design choices for the two IFE reactor plant designs. The engineering details for the systems and subsystems are presented to describe the expected performance and operation of the complete reactor plants.

6.1 Introduction

Chapter 4 described the rationale for the major subsystems which influence the overall plant design. Early identification of key plant design options was critical in the design process. Subsequently, effort was directed toward the development of the conceptual design of systems and subsystems to integrate plant requirements .

Even though many of the key system options has been chosen with the expert judgement of the team and the aid of the systems code, each design team did not have sufficient knowledge to independently begin to design the optimal system. Moreover, a collection of individual optimal system designs may not prove to represent the overall optimal plant design. As the system designs began to evolve, systems performance and cost modeling was incorporated into the systems code to improve the modeling fidelity. Then the systems model was exercised to examine the available parameter space and determine micro or macro changes in the design configuration and operating parameter space. This process was iterated many times throughout the course of the study. However, not all the decisions could be quantified by the systems model, rather some decisions were based on qualitative judgements regarding the merits of safety, environmental attractiveness, reliability, and design conservatism.

One of the popular misconceptions held by the fusion community prior to this study was that the physical separation of the IFE driver from the reactor cavity implied nearly complete design independence for all the major systems. This study found that there is a profound amount of interaction among all the systems. The type of target influences driver illumination scheme, beam quality, fuel cycle, and cavity design. The wall protection choice affects energy conversion efficiency, waste handling capability, beam propagation across the cavity, and so on. Physical separation affords many benefits and design freedoms, however there are still significant and strong interactions among the systems which must be accommodated.

The system designs documented in this chapter constitute a conceptual design for a KrF laser reactor power plant and a heavy ion laser reactor power plant. Section 6.2, Design Point Selection discusses the development and evolution of the two respective design points. That section also contains high level parameter lists for the two reactors. More detailed parameters lists are presented in Appendices A and B. The overall reactor and plant configurations are presented in Section 6.3 along with a discussion of the design integration of the major systems. The maintenance approach and RAM analyses are also discussed . Following are the sections explaining the designs and analyses for the individual plant systems. This chapter concludes with a discussion of the rationale for the selection of the major materials used in the designs, principally the reactor cavity with the high radiation environment. There is a significant discussion of the safety and environmental analyses conducted during this study. The final section is an assessment of the economic analyses conducted for the two designs. A detailed cost basis is provided in Appendix C.

6.2 Design Point Selection

The selection of an optimum operating point in parameter space for inertial fusion power plants involves a trade-off between target gain G as a function of driver output energy E_D, the driver efficiency η, and the change in driver cost with output energy. The basis for this is illustrated by the simple power flow diagram shown in Figure 6.2-1. In this figure the driver power is related to the output energy through the pulse repetition rate RR, namely $P_D = RR\ E_D / \eta$. The thermal power depends on the effective energy multiplication in the blanket $M' = 1 + f_n(M-1)$ where f_n is the neutron fraction of the fusion power. To simply power the driver, the product of the driver efficiency and target gain ηG must satisfy the following relation $\eta G > 1 / \varepsilon M'$. Net power generation requires ηG in excess of $1 / \varepsilon M'$, typically by a factor of two or more. An advanced thermal conversion efficiency of 40% and effective blanket multiplication of 1.1 thus imply a minimal ηG of ~5 for economic power generation. If the driver efficiency is 5%, a target gain greater than 100 is required. If the driver efficiency improves to 20%, a gain greater than 25 will suffice.

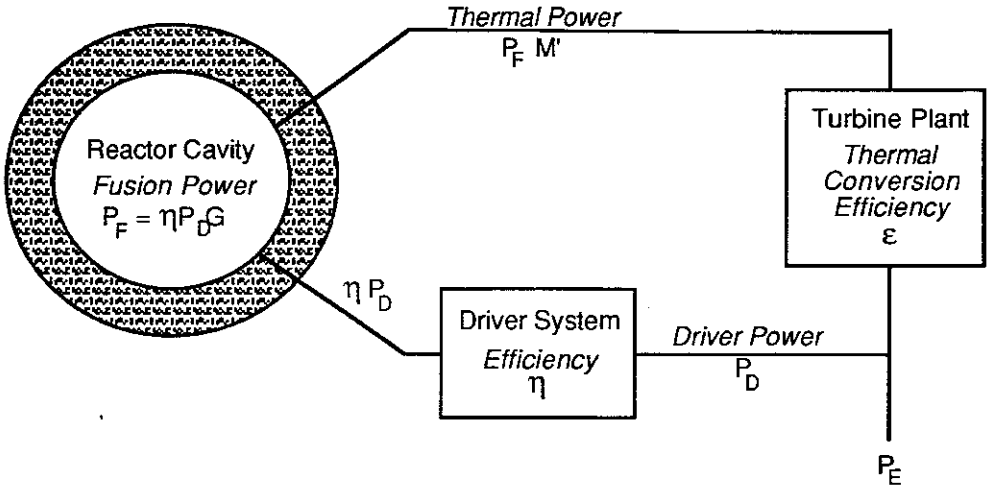

Figure 6.2-1. Simple Power Flow Diagram for an Inertial Fusion Power Plant

Systems modeling provides a basis for deciding how large an ηG is economically warranted. Typical target gain curves increase with driver output energy. Improved ηG is thus provided by increasing driver energy, but this implies a more costly driver. For a fixed-size plant, however, there can be a net cost savings because the driver is pulsed less frequently and therefore requires less input power. The size, hence cost, of the supporting plant equipment (reactor, steam generators, turbines, etc.) is thus reduced. The systems code quantifies this trade-off by parametrically modeling the size and cost of all major power plant systems. Incremental driver cost can then be weighed against the cost savings provided by higher target gain to determine the optimum size driver for the anticipated target gain curves.

This brings up an important point, namely that this process is intimately tied to the scaling of target gain with driver output energy. Gain curves for the present study were provided by a DOE-appointed Target Working Group (TWG). The TWG endeavored to level the technical optimism between the various laser illumination concepts (direct drive constant spot - CS, direct drive zoomed spot - ZS, and indirect drive - ID) and the indirect drive heavy-ion targets. For the laser driver, they provided their recommendations in the form of upper and lower bounds on the expected gain as a function of incident driver energy for each option. The TWG recommended an arithmetic mean of the upper and lower bound as a baseline gain curve for system studies that is represented by the constant spot curves. Figure 6.2-2 shows the resulting baseline gain curves for the KrF laser-driven target options.

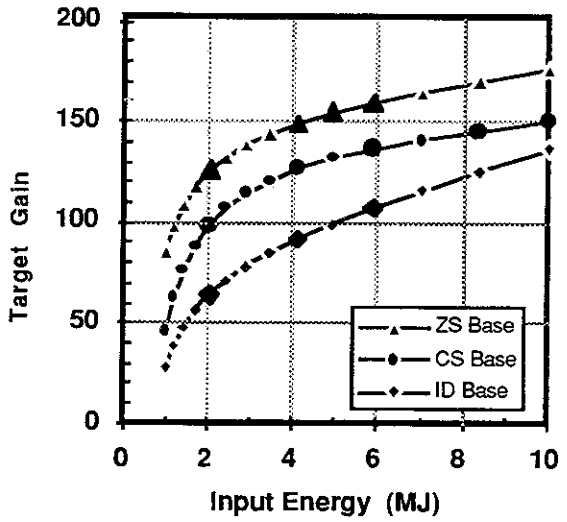

Figure 6.2-2. Baseline Gain Curves for KrF Laser Driver

The shape and magnitude of these curves directly influence the design point selection as discussed in the next section. The position of the ignition cliff ~2 MJ determines the minimum driver size whereas the slope of the curves determines the attractiveness of going to higher driver energy to improve ηG. Alternate target designs with different gain characteristics could push the design point to a different driver energy. This possibility is discussed in more detail in Section 5, Critical Issue 1, where economic considerations are used to determine the gain space region of interest for a smaller-size (100 MWe) power demonstration unit. It should also be noted that the significant disparity between the driver energy needed to achieve gain of ~100 for direct and indirect drive was the key reason that a direct-drive approach was selected for the present study. This is discussed in more detail in Section 4.6.

A final aspect of the systems modeling involves the fact that the code evaluated projected performance and cost between subsystems that in many cases employ technologies at vastly different stages of development. Efforts were made to normalize the cost projections across subsystems, but this is difficult where comparable hardware does not exist today. Costs were normalized to assumptions made for

recent MFE reactor studies[1-2] to provide a common basis for comparison. Elsewhere, costs were based on the best judgment of system experts. The economic scaling in the present systems model ICCOMO has evolved over many years. The models were originally developed as part of the STARFIRE reactor design study[3] and were adapted to IFE as part of the HIFSA project.[4] All cost models were updated to conform with the economic guidelines discussed in Section 3. A detailed description of the final cost models is presented in Appendix C.

The study guidelines indicated that costs are to be evaluated for a tenth-of-a-kind power plant. The study has conformed to this guideline and the rationale for doing so is presented in Appendix C. However, technology development will not be dictated by projected tenth-of-a-kind costs but rather by those for the first-of-a-kind system. The trade studies presented in this section include no learning curve adjustments—only first-of-a-kind costs. The results are therefore presented in the form of relative comparisons in order to avoid confusion in relating them to the tenth-of-a-kind costs discussed elsewhere.

6.2.1 Laser System Trade Studies - The Prometheus-L design point is the result of a number of different trade studies. These studies are summarized in Table 6.2.1-1. Many of these studies were evaluated within individual subsystems,

Table 6.2.1-1. Summary of Design Options Considered for KrF Laser System

Parameter	Baseline Value	Options/Range Considered
Target:		
Type	Direct Drive	Indirect Drive
Gain Curves	Average of Optim & Conserv	Optimistic, Conservative
Gain Curves	Average of Optim & Conserv	Zoomed Spot
Number Beams	60	30-90
Illumination	Tangential Focus	Nested Focus
Incident Energy (MJ)	4	2-8
Reactor Cavity:		
Wall Protection	Wetted Wall (Lead)	Dry Wall with Fill Gas
Breeder	Li_2O	FLiBe; LiPb Eutectic
Thermal Cycle (He Coolant)	Advanced Rankine	Direct Brayton
Coolant Pressure (MPa)	1.5	1-5
Driver System:		
Laser Amplifier	Electric Discharge with Raman Accumulator	Large Area E-Beam Pumped
Pulse Compression	Stimulated Brillouin Cell	Angular Multiplex, Hybrid
Amplifier Energy (kJ)	5.6	3-10
Amplifier Run Time (ns)	250	200-500
Optical Fluence (J/cm^2)	10	3-10
Final Mirror:		
Type	Grazing Incidence Metal on Ceramic Structure	Grazing Incidence Metal on Metallic Structure
Protection	Distance; Residual Gas; Deflection Magnets	Shutters; Cover Gas; Gas Prism

however, some trades could not be quantified within a subsystem. The systems code was used to resolve these trade-offs. The trade studies directed at choosing between technology options (e.g., indirect versus direct drive targets, single versus multiple beam LINAC, etc.) are discussed in Section 4. The discussion presented in this section concerns itself only with the rationale for selecting a certain operating range in parameter space for the baseline technology options.

In addition to design point selection, studies were also performed to assess the sensitivity of the overall performance to various subsystem technology assumptions, e.g., discharge laser intrinsic efficiency and output energy, optical damage limit, number of beamlines, etc. These studies indicate which research and development areas have the most leverage and thus might be considered the most critical.

Laser Design Point Selection and Sensitivity Studies - A 4 MJ driver energy was selected for the Prometheus-L design point based on the trade study summarized in Figure 6.2.1-1. This figure shows the relative driver capital cost, COE, and pulse repetition rate as a function of driver energy for the reference NLO driver architecture. The projected COE reaches a minimum at 4 MJ and rises slowly thereafter. As Figure 6.2-2 illustrates, the flatness of the direct-drive gain curves above the ignition cliff makes it unattractive to pay for the extra driver needed to achieve higher gains. In fact, a 3 MJ driver is projected to have performance nearly identical to the baseline system. The 4 MJ system was selected because the higher 8.2 pps repetition rate at 3 MJ was thought to provide inadequate time for reducing the lead vapor pressure in the cavity back to the 1-3 mtorr level required to prevent laser-induced gas breakdown. Cavity clearing was a key concern in the design of the Prometheus-L system as discussed in Section 6.8.

Figure 6.2.1-2 shows the sensitivity of the Prometheus-L design to key assumptions about the driver performance. The data displayed in the figure is summarized in Table 6.2.1-2 together with the parameters which were varied and their range of variation. In determining the change in COE, only the indicated parameter was allowed to vary, all other parameters were held constant. In many instances the change in COE could be offset to some extent by reoptimizing the overall design for the new conditions. For example, the lower gain predicted for the conservative curve would likely lead to the selection of a higher driver energy but this was not factored into the sensitivity study.

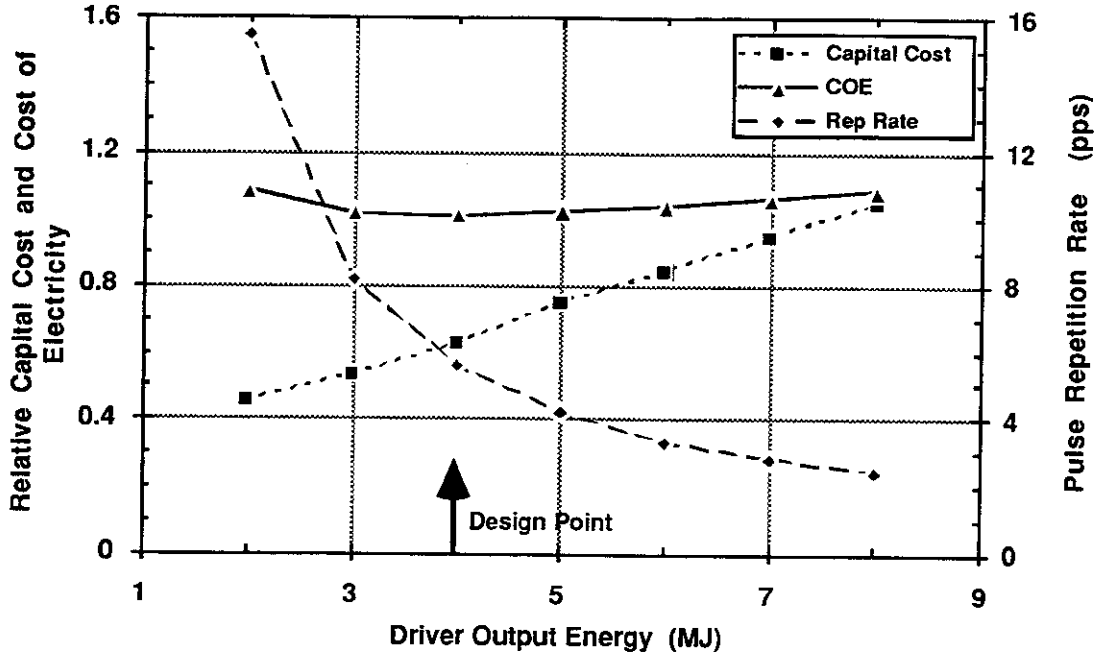

Figure 6.2.1-1. Scaling of Prometheus-L Driver Capital Cost, COE, and Pulse Repetition Rate with Driver Output Energy

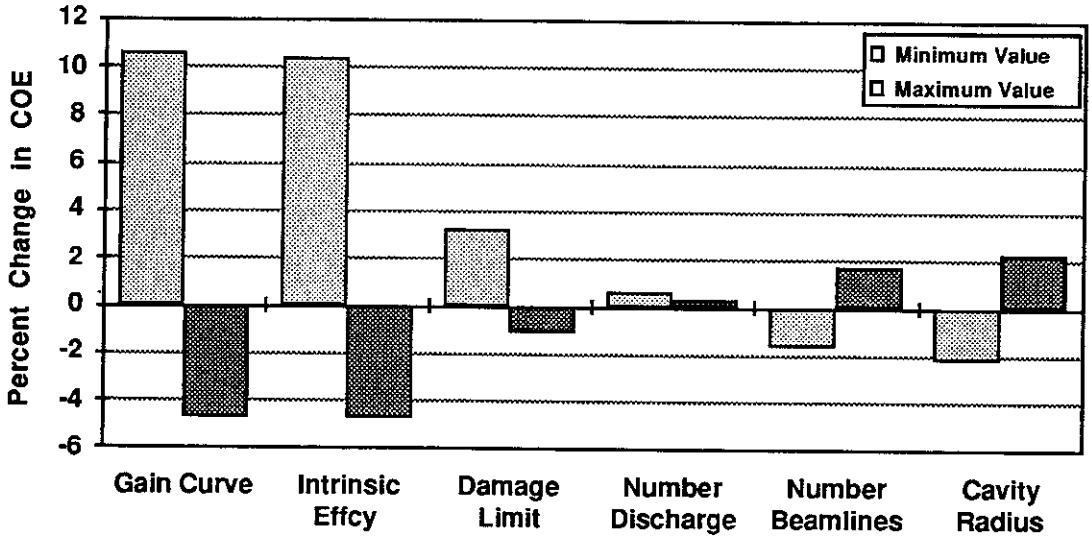

Figure 6.2.1-2. COE Sensitivity to Prometheus-L Design and Performance Assumptions

Table 6.2.1-2. COE Sensitivity to Variations in Key Prometheus-L Design Parameters

Parameter	Baseline Value	Minimum Value	Change in COE (%)	Maximum Value	Change in COE (%)
Gain Curve (Consvrt, Optm)	126	86	+10.6	165	-4.8
Laser Intrinsic Efficiency (%)	15	10	+10.3	20	-4.7
Optical Damage Limit (J/cm^2)	10	5	+3.2	15	-1.1
Num Dischg Lasers, Energy (kJ)	960, 6	240, 20	+0.6	2160, 2	+0.3
Number Final Beamlines	60	30	-1.7	90	+1.7
Cavity Radius (m)	5	4.5	-2.2	5.5	+2.3

Figure 6.2.1-2 also shows that COE depends most strongly on the gain curve assumption and the discharge laser intrinsic efficiency. The projected COE is 10% higher at the minimum value considered for these two parameters and drops 5% below the baseline value at their upper limit. These are sensitive parameters because there is very little ηG margin for the KrF laser driver since the overall efficiency is only 6.5%. Lowering the optical damage limit to 5 J/cm^2 causes a 3% increase in COE, while raising it to 15 J/cm^2 only decreases COE by 1%. There is thus little incentive to improve optical coatings beyond the 10 J/cm^2 point. COE is virtually independent of the discharge laser output energy even though the number of discharge lasers varies from 2160 down to 240. This is because the lasers are producing the same amount of total energy (4 MJ) in either case. Hence, the pulsed power energy requirement is the same and it is the major cost driver. Finally, a decrease in the number of beamlines from 60 to 30 or a reduction in cavity radius from 5 to 4.5 m would each lower COE by 2%. Conversely, COE would increase by 2% for 90 beamlines or if a 5.5 m cavity radius was needed to lower cavity vapor pressure.

6.2.2 Heavy Ion System Trade Studies - The Prometheus-H design point is based on a number of trade studies. These studies are summarized in Table 6.2.2-1. The heavy-ion driver has more scaling flexibility because it produces the requisite total energy by combining several ion beamlets at a discrete kinetic energy. The choice of ion charge state and kinetic energy lead to significant differences both in the accelerator configuration and in the target performance which must both be considered in determining the optimum design point. This section discusses these issues along with the results of sensitivity studies which were run to document the leverage of key design parameters on the overall system performance. Table 6.2.2-1 also highlights several trade studies which are discussed elsewhere in this report. The rationale for choosing a single versus multiple beam LINAC is presented in Section 4.1. The rationale for selecting a self-formed channel for cavity transport and the resulting target focal spot size and channel energy coupling is presented in Section 4.3. Finally, the rationale leading to the choice of a wall protection scheme identical to that for the laser system is presented in Section 4.4 and a discussion of target issues for the heavy ion system is presented in Section 4.6.

Table 6.2.2-1. Design Options Considered for Heavy Ion System

Parameter	Baseline Value	Options/Range Considered
Target:		
Type	Indirect Drive	
Ion Range (g/cm^2)	0.045 (4 GeV Lead)	0.025-0.2
Spot Size, Radius (mm)	3	2-5
Illumination	Two Sided	One Sided
Incident Energy (MJ)	7	4-9
Final Beam Trnsp Effncy (%)	90	70-100
Reactor Cavity:	Wetted Wall (Lead)	Same as Laser System
Driver System:		
LINAC Type	Single Beam with Storage Rings	Multiple Beam
LINAC Scaling	$\alpha = 0.2$; $\kappa = -0.15$	$\alpha = (0.2 - 0.5)$; $\kappa = (-0.2 - 0.0)$
Ion Type	+2 Lead	+1 to +3 Lead
Ion Energy (GeV)	4	4-8
Focusing Quads	Superconducting	Normal
Cavity Transport	Self-formed Channel	Ballistic; Pre-formed Channel

Figure 6.2.2-1 shows the gain curves provided by the TWG for the heavy ion system. These gain curves illustrate the strong influence which both beam spot size and ion energy have on the overall system performance. For a 7 MJ system with a 3 mm radius focal spot, the gain drops from ~100 at an ion kinetic energy of 2.4 GeV to 50 at 12.5 GeV. With a 4 mm radius spot, the change is even more dramatic going from a gain of 90 at 2.4 GeV to no gain at all. These large changes in gain, hence ηG, have a significant impact on the overall system performance which is a key aspect of the heavy ion trade studies.

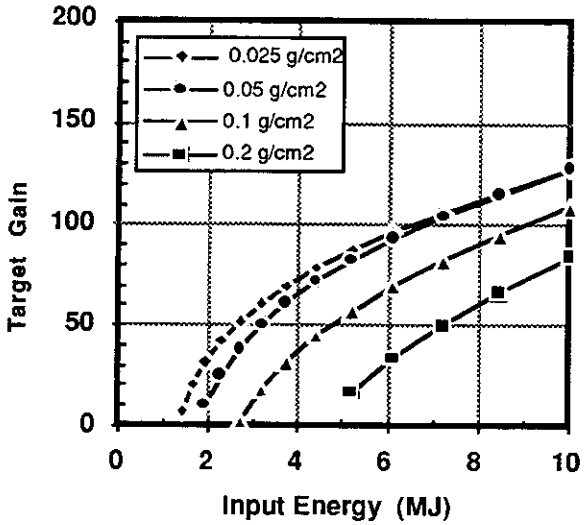

Figure 6.2.2-1. Baseline Gain Curves for Indirect-Drive, Heavy Ion Targets With a 3 mm Radius Focal Spot.

The systems code permits this gain variation to be traded off against the driver cost which tends to increase with ion energy. Figure 6.2.2-2 shows how LINAC size, cost and complexity scale with ion energy for a 7.8 MJ, single beam system operating at 5 pps. It shows that cost increases with ion energy because the LINAC length grows from 2200 m (1210 quads) at 4 GeV to 4200 m (1682 quads) at 8 GeV. The number of focusing quads is a significant cost factor. As a result, the lower energy system is favored from a cost standpoint in spite of the fact that more pulses per beam hence storage rings are required at 4 GeV (34 as compared to 18 at 8 GeV). This cost advantage must be weighed against the added technical risk of storing the beams for a longer time and the added complexity of the storage ring, final transport and final focus systems. System efficiency is also lower at 4 GeV (14.7% as compared to 16.6% at 8 GeV) because the induction cores are recycled more times per pulse. The Prometheus-H design point was chosen based on all these considerations.

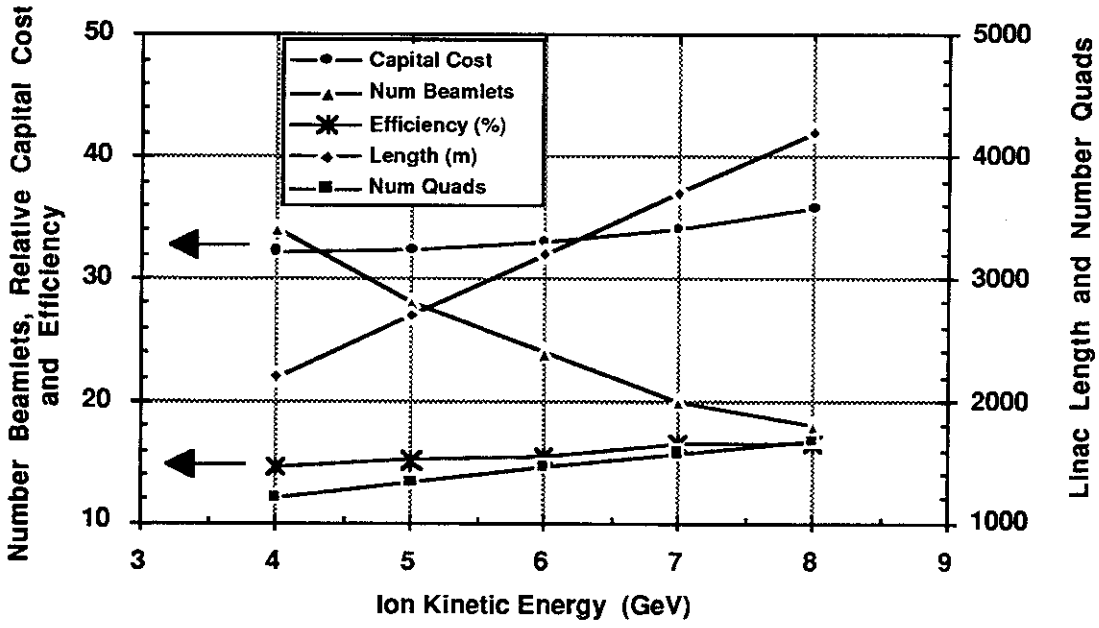

Figure 6.2.2-2. SB LINAC Size and Cost Scaling Vs. Ion Energy for a +2 Lead, 7.8 MJ and 5 pps System With Lee Lattice Scaling.[5]

One of the main induction LINAC design challenges involves the space charge limit on transportable current in a periodic focusing lattice. This limit necessitates multiple transport channels (typically > 10 beamlets) for heavy ion fusion drivers. Past systems studies[4] have envisioned a multiple beamlet lattice consisting of a closely packed quadrupole bundle surrounded by massive induction cores. The Prometheus-H design considers an alternative approach consisting of a single beam transport lattice coupled with intermediate storage rings to accumulate the required number of beamlets. In either case there is significant motivation to reduce the number of beamlets as much as possible in order to simplify the system design. Figure 6.2.2-2 shows that one way to reduce the number of beamlets is by increasing the ion energy. Unfortunately, this has an adverse effect on gain. In fact, Figure 6.2.2-1 shows that the

gain curves motivate the LINAC designer to work towards an ion energy of 4 GeV or less for lead ions. Design trade studies thus focused on alternative transport lattice configurations that would minimize the number of beams for a 4 GeV system.

The transport lattice scaling used for these trade studies is based on the following relations suggested by Maschke.[6] In these relationships, V is the local accelerator column voltage and I is the local individual beamlet current. These relations are used to define the number of beamlets N_B; the mean beam radius a; the space charge depressed phase advance per lattice period (depressed tune) σ; the beamlet bunch length $\delta = \tau\beta c$; and the number, length, and location of the focusing quads which are specified in terms of the lattice period 2L and the magnet occupancy (packing) fraction per lattice period η. In addition, several constraints based on physical limitations must be satisfied along with the relationship between beam energy and total charge.

Maschke[6] characterized the transport lattice scaling with LINAC voltage in terms of two parameters α and κ as summarized in Table 6.2.2-2. Lattice scaling suggested by Ed Lee[5] is a special case of this general parameterization as indicated where $\alpha = 0$, $\kappa = -1/4$ in the ramped gradient and $\alpha = 1/2$, $\kappa = 1/8$ in the fixed gradient sections.

Table 6.2.2-2. Prometheus-H Transport Lattice Scaling Model

Parameter	Maschke Scaling	Ed Lee Scaling[5] Ramped	Ed Lee Scaling[5] Fixed	Final Transport Scaling
Lattice Half Period, L	$V^{\alpha-\kappa}$	$V^{1/4}$	$V^{3/8}$	$I^{\zeta-1}$
Depressed Tune, σ	V^{κ}	$V^{-1/4}$	$V^{1/8}$	$I^{-\zeta}$
Beam Radius, a	$V^{\alpha/2-\kappa-1/4}$	Const	$V^{-1/8}$	$I^{\zeta-1/2}$
Bunch Length, δ	$V^{\alpha-1/2}$	$V^{-1/2}$	Const	$I^{\zeta-1}$
Packing Fraction, η	$V^{-3\alpha/2+\kappa+1/4}$	Const	$V^{-3/8}$	$I^{3/2-\zeta}$

The additional constraints involve the space charge limit on transportable current:

$$I_{max} = \frac{Q}{\tau N_B} = 1.56 \times 10^7 \sigma_o^2 \left(\frac{a}{2L}\right)^2 \left(\frac{A}{Z}\right)(\beta\gamma)^3, \qquad 6.2.2\text{-}1$$

where I_{max} is in amps, $Q = 10^6 Z E_B/E_{ion}$ is the required charge in coulombs (E_B in MJ and E_{ion} in GeV), A and Z are the ion atomic mass and charge state, and τ is the pulse length. The relation between normalized emittance $\varepsilon_n = \beta\gamma\varepsilon$ and phase advance:

$$\varepsilon_n = \sigma\left(\frac{a^2}{2L}\right)(\beta\gamma). \qquad 6.2.2\text{-}2$$

The relation between undepressed phase advance σ_o and the focal lattice properties:

$$\sigma_o = B_P\left(\frac{\eta a}{[B\rho]L^2}\right), \qquad 6.2.2\text{-}3$$

where B_P is the poletip field and $[B\rho] = 3.13\,\beta\gamma\left(\frac{A}{Z}\right)$ is the beam rigidity in T-m. (The poletip field is actually the magnetic field at the edge of the beam, so the maximum

field in the magnet is typically 1.5 to 2 times higher.) The relation governing the maximum rate that the voltage gradient can be increased in the ramped gradient section:

$$\frac{dV}{dx} \le 0.25\left(\frac{V}{\delta}\right)\left[\frac{1}{2} - \frac{V}{\delta}\left(\frac{d\delta}{dV}\right)\right]^{-1}. \qquad 6.2.2\text{-}4$$

And finally the practical limits on quadrupole packing fraction in the lattice $\eta < 0.80$ and quadrupole aspect (bore to length) ratio $a/\eta L < 0.25$.

These scaling relations are implemented by choosing values for the lattice scaling parameters with voltage along the LINAC α and κ, and with beamlet current I in the final transport (typically $\zeta = -0.8$). The undepressed phase advance $\sigma_o = 80°$ maximum poletip field $B_{PT} = 3$ T, desired final transport section length (typically 180 m), pulse length at the target (typically 7-8 ns), beam and ion energies are also specified. The code then searches for a number of beamlets and bunch length at the high energy end of the LINAC that do not violate the packing fraction and aspect ratio limits at either the injector end or in the final transport section where beamlet current increases rapidly due to bunching. If the constraints cannot be satisfied, the poletip field is reduced. The poletip field is typically reduced to ~2T before a solution is found for the combinations of α and κ considered here.

An examination of Table 6.2.2-2 shows that some combinations of α and κ are more attractive than others and the trade studies discussed here focus on them. Initial studies considered the Lee[5] choice for lattice scaling and these results were used in Figure 6.2.2-2. However, this scaling results in 34 beamlets at 4 GeV for a 7 MJ driver which presents a significant technical and design challenge both in the storage rings and the final focus. One logical alternative scaling involves setting $\alpha = 0.5$ and $\kappa = 0$. This is attractive because it leads to a common quadrupole size (a and ηL are both constant) down the entire length of the LINAC. Another alternative involves simply holding magnet bore size constant down the length of the LINAC, i.e., choosing $\kappa = \alpha/2 - 1/4$. The quadrupole length will vary for this family of scaling possibilities, but discrete steps can be provided by adjusting the magnet field strength slightly. It furthermore is desirable to have $\alpha < 0.5$ so that the magnet aspect ratio ($a/\eta L$) decreases along the LINAC to avoid problems with aberrations. This leads to values of $\kappa < 0$ which corresponds to letting the phase advance float downward along the LINAC length. This leads to a worst case final phase advance of 2.2° assuming $\sigma = 8°$ at the injector end, which should not be a problem.

Table 6.2.2-3 summarizes the results of these trade studies. The number of magnets is significantly reduced for $\alpha = 0.5$, from ~1200 for the Lee cscaling[5] to 356. Unfortunately, the number of beamlets nearly doubles, going from 34 to 66. This in

Table 6.2.2-3. Summary of LINAC Lattice Scaling Trade Studies for a 4 GeV, 7.8 MJ, +2 Lead System

Lattice Scaling		Number	Number	Final Pulse	Final Phase	Overall Driver System	
Alpha	Kappa	Beamlets	Quads	Length (ns)	Advance (deg)	Effcy (%)	Cost (M$)
0.50	0.00	66	356	150.0	8.0	7.50	765.0
0.40	-0.05	36	484	150.0	5.8	11.55	619.9
0.30	-0.10	18	760	150.0	4.2	18.05	645.1
0.20	-0.15	16	956	89.8	3.0	21.54	595.0
0.10	-0.20	38	982	18.3	2.2	17.05	447.6

turn lowers the overall efficiency to 7.5% due to increased induction core losses. The α=0.5 scaling was thus rejected for the final design point. However, the table shows that more attractive results occur as α is reduced from 0.5 to 0.2. The number of beamlets decreases from 66 to 16, the efficiency improves from 7.5 to 21.5% and the cost drops from $765 to $595 M. The cost trend continues for α = 0.1, but the other trends reverse. The turnaround is a result of the rapid drop in final pulse length that is required to prevent violating the quadrupole packing fraction constraint in the final transport section for values of α < 0.2. Based on this result, transport lattice scaling using α = 0.2 and κ = -0.15 was selected for the baseline design point.

To this point, the discussion has focused on the selection of LINAC parameters that minimize the number of beamlets for a given total output energy. An energy of 7.8 MJ was used for illustration purposes because it was selected for the Prometheus-H driver. This accounts for a 10% loss in the process of forming the cavity transport channel and coupling the driver output energy through the channel into the target as discussed in Section 6.5. Hence only 7 MJ of energy is actually assumed to be available for producing target gain. Figure 6.2.2-3 depicts the basis for selecting this driver energy. It shows that the projected COE has yet to reach a minimum at 9 MJ for the selected LINAC design configuration. The projected incremental driver cost for the single beam LINAC and the slope of the heavy-ion gain curves favor higher energies. The number of beamlets was originally a concern at this energy, more than 50 were anticipated for a 4 GeV system, however this concern is mitigated somewhat by the alternative lattice transport scaling which is projected to need only 22 beamlets at 9 MJ. Nevertheless, higher energy drivers certainly represent a greater development challenge both for the driver and the cavity with must withstand a higher yield. This realization coupled with the marginal improvement in COE above 7 MJ still justify it as a design point.

It is worthwhile here to note that the alternative lattice transport scaling really opens a more attractive heavy ion LINAC design window that previously was not accessible due to the large number of required beamlets. This can be understood by referring to the gain curves as shown in Figure 6.2.2-1. The gain falls off rapidly for ion energies above 5 GeV and is almost a factor of 2 lower for the 10 GeV ions typically proposed

in the past. In addition, lower energy ions are much less sensitive to variations in focal spot size. This is quantified in Table 6.2.2-4 which summarizes the sensitivity of COE to variations in key driver performance parameters.

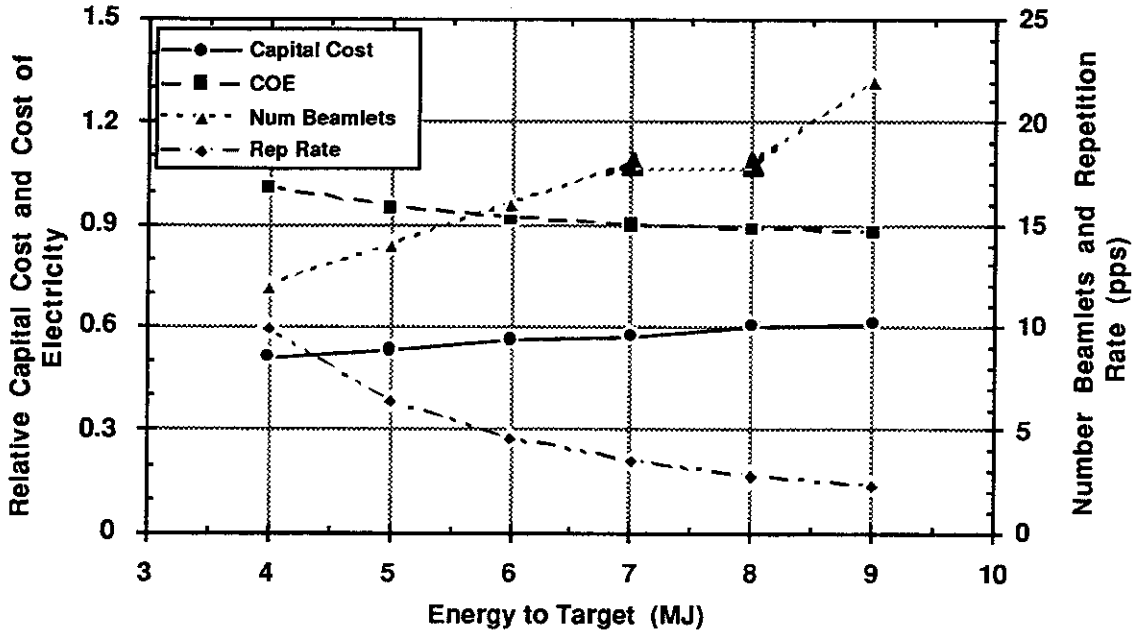

Figure 6.2.2-3. Scaling of Prometheus-H Driver Cost, COE, Repetition Rate, and Number of Beamlets with Output Energy

Table 6.2.2-4. COE Sensitivity to Variations in Key Prometheus-H Design Parameters

Parameter	Baseline Value	Minimum Value	Change in COE, Effcy*	Maximum Value	Change in COE, Effcy*
Focal Spot Radius (mm)	3	2	-2.1	4	+3.6
Spot Radius Change at 7 GeV**	3	2	-4.3	4	+8.6
Final Beam Transport Effcny (%)	90	80	+0.8	100	-0.6
Ion Kinetic Energy (GeV)	4	3	-2.7, -13.0	7	+18.2, +21.4
Core Flux Swing (T)	1.5	1.0	+1.7, +8.4	2.0	+0.1, -9.3
Ion Charge State	+2	+1	+24.5, +2.8	+3	-4.2, -4.4

* Change in driver efficiency is indicated only for parameters that influence it significantly

** Changes are normalized to 7 GeV system with 3 mm radius spot which is 18% higher than 4 GeV COE

These results highlight several key aspects of the Prometheus-H driver design. The primary one involves the improved cost and performance characteristics provided by the reduced ion kinetic energy. As is indicated, COE is 18% higher for a 7 GeV design due to the increased length of accelerator required at this energy. The number of beamlets is reduced from 18 to 6 at 7 GeV , but the single beam approach, coupled with the alternate transport scaling, eliminates most of the complication (hence cost) of

added beamlets at 4 GeV. The results also indicate that there is little motivation to further reduce beam energy. COE is 3% lower at 3 GeV but 32 beamlets are required at this energy which complicates the final transport and lowers driver efficiency by 13%.

An added benefit of the lower ion energy is reduced sensitivity to target gain curve characteristics. The results show that a 7 GeV system is twice as sensitive to spot size variations as the 4 GeV design point. This is important because it minimizes the effect which the poorly understood transport channel re-imaging properties may have on system performance. Insensitivity to transport channel properties is reinforced by the weak COE dependence on target coupling efficiency (beam energy loss in the transport channel). A doubling of energy loss (from 10 to 20%) would only increase COE by 1%. The results also indicate very weak COE dependence on Metglas flux swing. A low flux swing of 1.5 T was selected for the baseline design to reduce induction core energy losses since this was thought to be a key factor in the design of a single beam LINAC where the cores are recycled several times per pulse. Indeed, the driver efficiency changes by ±9 % as flux swing is varied from 1 to 2 T, however this causes only a 1 % change of COE. Finally, the results highlight that there is still a significant advantage to higher charge states for the single beam system, but that the payoff is limited beyond +2. The cost of electricity is 24 % higher for singly charged ions while it drops by 4 % for charge state 3. Unfortunately, the number of beamlets increases to 36 for +3 ions which may offset the indicated cost advantage once the engineering details of final transport and focusing are evaluated.

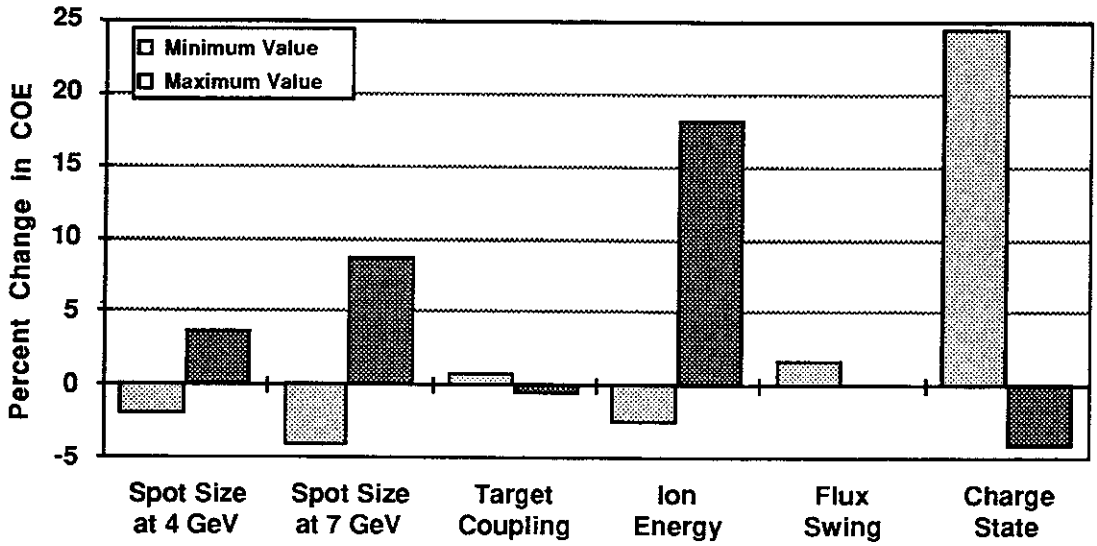

Figure 6.2.2-4. COE Sensitivity to Prometheus-H Design and Performance Assumptions

References for 6.2

1. F. Najmabadi, R. W. Conn, et al., "The ARIES-I Tokamak Reactor Study, Final Report,", UCLA-PPG-1323, 1991

2. M. A. Abdou, "FINESSE, A Study of the Issues, Experiments and Facilities for Fusion Nuclear Technology Research & Development," PPG-821, UCLA-ENG-84-30, 1984.

3. C. C. Baker, M. A. Abdou, et al., "STARFIRE - A Commercial Tokamak Fusion Power Plant Study," ANL/FPP-80-1, September 1980.

4. D. S. Zuckerman, et al., "Induction LINAC Driven Heavy Ion Fusion System Model," Fusion Technology, Vol. 13, #2, 1986.

5. Dr. Edward Lee, Lawrence Berkeley Laboratory, Personnel Communication, 1991.

6. Mr. Alfred Maschke, TRW, Personal Communication, 1991.